Applied Surface Science 491 (2019) 750–756

Contents lists available at ScienceDirect

Applied Surface Science

journal homepage: www.elsevier.com/locate/apsusc

Full length article

Transition metal-doped janus monolayer SMoSe with excellent thermal spin filter and spin Seebeck effect

Guangqian Ding[a,*], Mian Wei[a], Gokhan Surucu[b,c,d], Zhengyong Liang[a], Xiaotian Wang[e,*]

[a] School of Science, Chongqing University of Posts and Telecommunications, Chongqing 400065, China
[b] Department of Physics, Middle East Technical University, 06800 Ankara, Turkey
[c] Department of Electric and Energy, Ahi Evran University, Turkey
[d] Photonics Application and Research Center, Gazi University, Turkey
[e] School of Physical Science and Technology, Southwest University, Chongqing 400715, China

ARTICLE INFO

Keywords:
Janus monolayer SMoSe
Density functional theory
Thermal spin transport
Spin filter effect
Spin Seebeck effect
Transition metal

ABSTRACT

Motivated by the recent experimental synthesis of the novel janus monolayer SMoSe, we propose the design of spin caloritronic material based on transition metal-doped SMoSe monolayer. Using density functional theory combined with the non-equilibrium Green's function method, we show that a perfect thermal spin filter and a negative differential thermoelectric resistance are obtained in Fe-doped SMoSe janus monolayer. For Cr-doped SMoSe janus monolayer on the other hand, the thermal induced spin-up and spin-down currents flow in opposite directions with nearly equal magnitude, producing a perfect spin Seebeck effect. These important results are elucidated through the band structures and transmission spectrum. Our findings put forward an effective route to design spin caloritronic devices, which can be applied in the future to waste heat recovery and information technology.

1. Introduction

Spin caloritronics is a combination of spintronics and heat transport in a material, which aims at driving the spin current by a temperature bias instead of transverse electric field or gate voltage, providing an alternative strategy for waste heat recovery and low-power-consumption technology [1–4]. A notable achievement of spin caloritronics is the observation of the spin Seebeck effect (SSE) in a metallic magnet, in which the spin voltage and spin current are generated via a pure temperature bias [5–8]. To reduce the Joule heating brought about by the electron current as much as possible, it is necessary to produce pure spin current with inhibited charge current, which is usually called a perfect SSE. In addition to the SSE, another important effect of spin caloritronics is the thermal spin filter effect (SFE), a phenomenon in which temperature induced spin currents are inhibited in one spin channel while opened in another spin channel, which can be applied as a thermal controlled spin valve [9–12].

To further promote and utilize spin caloritronics, it is necessary to predict or design promising candidates for spin caloritronic materials. In recent years, the demand of electronic devices to be small-size and high-capacity has promoted the development of two-dimensional (2D) magnetic materials [13,14]. Since most 2D materials are non-magnetic, different technologies have been tried to induce magnetism in 2D materials. For example, Fu et al. [15] proposed a ferromagnetic silicene nanoribbon with single-hydrogen-terminated, while double-hydrogen-terminated silicene nanoribbon is antiferromagetic. They also showed that the hydrogen-terminated silicene nanoribbon heterojunction exhibits the SSE and thermal colossal magnetoresistance. Zou et al. [16] found that Fe-doped monolayer MoS_2 is a half-metal, which produces a perfect thermal SFE. More recently, theoretical prediction has shown that ferromagnetic γ-graphyne nanoribbon exhibits the SSE and rectifier and diode effects, and carbon substitution of boron or nitrogen in single-layer boron-nitrogen nanotubes generates remarkable SFE and SSE [17,18]. In addition, monolayer VTe_2 also shows SFE and SSE, as recently reported by Musle et al [19]. Generally, the key challenge of designing spin caloritronics devices with perfect SFE or SSE lies in how to control the thermal spin currents, which depends on the magnetism features of the alternative materials. Considering experimental feasibility, it is better to choose existing 2D materials as candidates for designing spin caloritronics devices.

Recently, janus monolayer (JM) transition-metal dichalcogenide SMoSe has been synthesized [20], where the top layer of Se atoms are substituted by S atoms by controlling the sulfurization of the monolayer $MoSe_2$, leading to a crystal configuration of a S-Mo-Se sandwich. This is

* Corresponding authors.
E-mail addresses: dinggq@cqupt.edu.cn (G. Ding), xiaotianwang@swu.edu.cn (X. Wang).

https://doi.org/10.1016/j.apsusc.2019.06.174
Received 9 April 2019; Received in revised form 16 June 2019; Accepted 17 June 2019
Available online 18 June 2019
0169-4332/

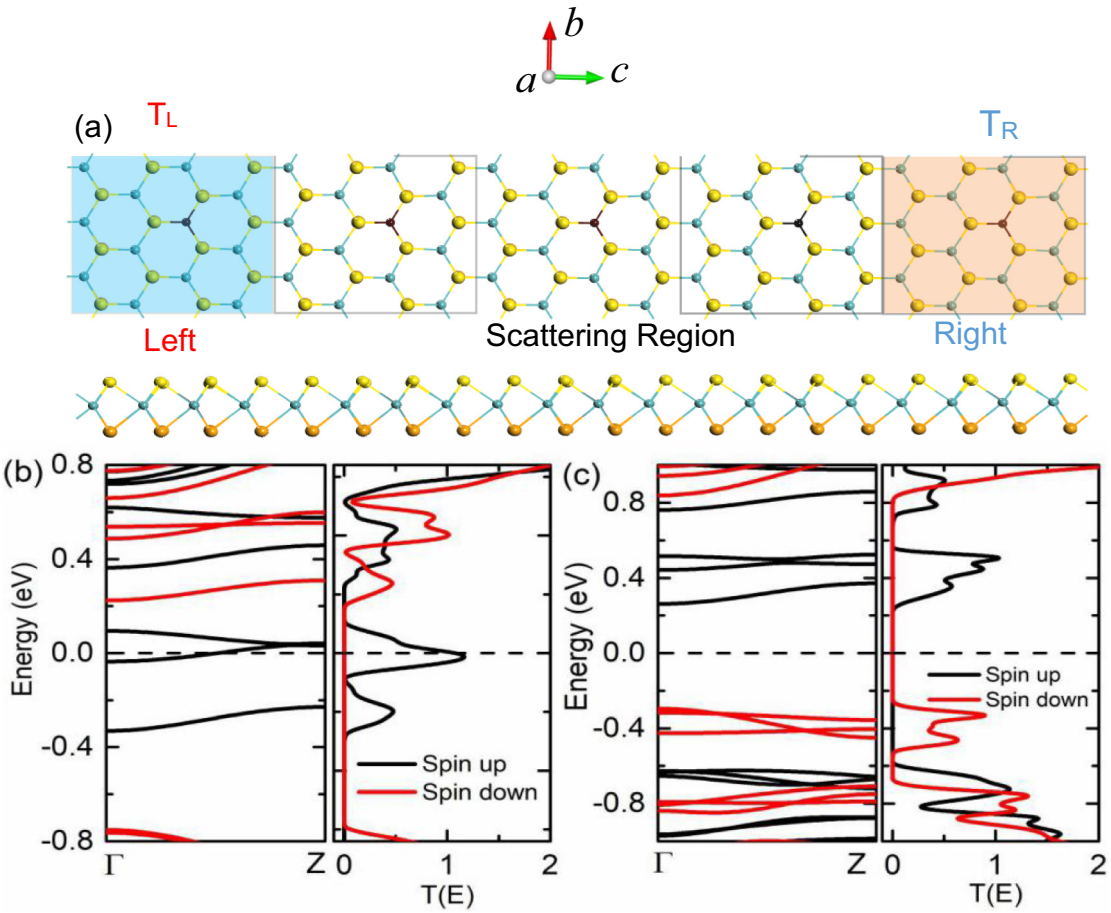

Fig. 1. (a) Schematic of the Fe(Cr)-doped SMoSe JM homo-junction with armchair configuration, in which the black, yellow, gray, and red atoms denote Fe(Cr), S, Mo and Se elements, respectively. The upper and under panels of (a) are the top and side view of the device. The left and right panels of (b) show the calculated band structure of the Fe-doped JM and the transmission spectrum of the homo-junction. Similarly, (c) shows the band structure of Cr-doped JM and the corresponding transmission spectrum of its homo-junction. (For interpretation of the references to color in this figure legend, the reader is referred to the web version of this article.)

a semiconductor with an indirect band gap of 1.478 eV. According to previous studies, substituting Mo with other transition metals can transform the semiconducting monolayers into magnetic ones [16,21–23]. Considering this, in this work, we design promising candidates for spin caloritronics materials via transition metal-doped SMoSe JM. We show that Fe-doped SMoSe JM is a ferromagnetic half-metal with a perfect thermal SFE and high spin current. For Cr-doped SMoSe JM, it behaves as a typical ferromagnetic spin semiconductor with a finite band gap, importantly, the symmetrical spin-up and spin-down transmission spectrum give rise to a perfect SSE. These findings may be helpful in the design of promising spin caloritronics devices.

2. Model and computational methods

Fig. 1(a) shows the doped SMoSe JM. The dashed square denotes the doped unit, in which one Mo atom is substituted by a Fe(Cr) atom in a $4 \times 4 \times 1$ supercell of SMoSe JM. A homo-junction is formed by repeating the doped unit along the transport direction *c*-axis. The source (left electrode) and drain (right electrode) are modeled using a semi-infinite replica of the doped unit along the transport direction. Three doped units were used as the scattering region. To eliminate interactions between adjacent layers, a 15 Å vacuum region is placed along the *a*-axis. During the calculation of thermal spin transport, the drain is set as the high-temperature side, while the source is the low-temperature side.

Structural relaxation is performed within the framework of density functional theory (DFT), using generalized-gradient-approximation (GGA) pseudopotentials and Perdew–Burke–Ernzerhof (PBE) exchange correlation functionals as implemented in the Vienna ab initio simulation package (VASP) [24,25]. The plane-wave cutoff is set to 500 eV. The reciprocal space is sampled by $15 \times 15 \times 1$ Monkhorst-Pack *k*-meshes, and the positions of the atoms are fully relaxed until the maximum force on each atom becomes smaller than 10^{-3} eV/Å. The convergence criterion of the self-consistent loop is set as 10^{-6} eV. Additionally, the Bader charges are computed using the VASP code, and the results are analysed using the algorithm developed by Henkelman et al. [26], which is based on Bader's approach [27].

The thermal spin transport properties are calculated using non-equilibrium Green's function (NEGF)/DFT methods, as implemented in the Atomistix ToolKit (ATK) package [28–30]. The spin-dependent PBE and SGGA functionals are adopted. A plane-wave cutoff of 150 Ry and a $1 \times 1 \times 100$ Monkhorst-Pack *k*-point grid are employed. Additionally, a Double-Zeta-Polarized (DZP) basis set is considered to obtain accurate results. According to the Landauer-Büttiker formula, the spin-dependent current through the device is given by the following equation [31,32]:

$$I^{\uparrow(\downarrow)} = \frac{e}{h}\int_{-\infty}^{\infty}\{T^{\uparrow(\downarrow)}(E)[f_L(E,T_L)-f_R(E,T_R)]\}dE, \quad (1)$$

where $T_{L(R)}$ and $f_{L(R)}$ are the temperature and Fermi-Dirac distribution of the left and right electrodes, respectively, and $T^{\uparrow(\downarrow)}(E)$ is the spin-dependent transport function, which can be calculated using the NEGF formalism in the linear-response regime as:

$$T^{\uparrow(\downarrow)}(E) = Tr\,[\Gamma_L G^R \Gamma_R G^A]^{\uparrow(\downarrow)}, \quad (2)$$

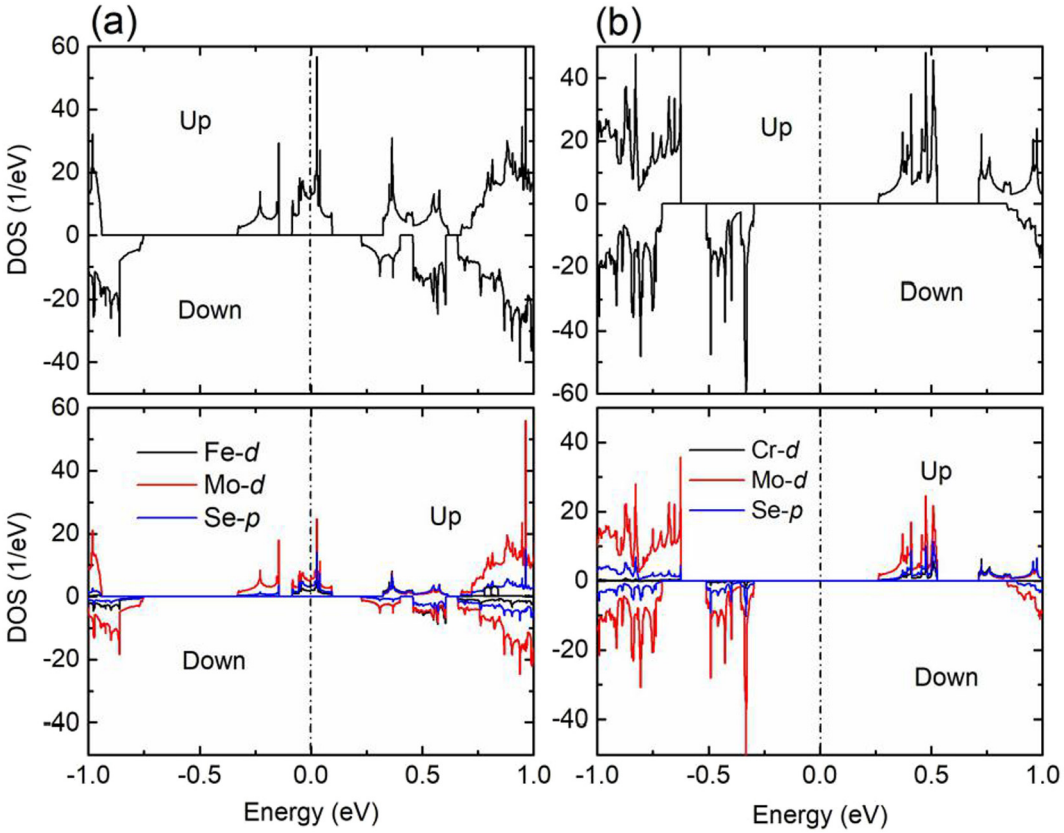

Fig. 2. The spin-dependent density of states and projected density of states of Fe-doped SMoSe JM (a) and Cr-doped SMoSe JM (b). The Fermi level is set at zero and labeled using a dashed line.

where $G^{R(A)}$ is the retarded (advanced) Green's functions of the scattering region, and $\Gamma_{L(R)}$ is the coupling matrix which indicates the interaction between the scattering region and the left (right) electrode.

3. Results and discussion

Fig. 1(b) shows the calculated band structure of Fe-doped SMoSe JM, and the transmission spectrum of its corresponding homo-junction. Previous studies have indicated that the transition metals doped MoS_2 monolayer are usually ferromagnetic [16,33,34]. In this work, our calculations show that Fe-doped SMoSe JM is also a ferromagnetic half-metal, with a total magnetic moment of $2\mu_B$ per doped unit cell. As can be seen in Fig. 1(b), the magnetic moment of this doped JM results from energy splitting between the spin-up and spin-down states in the vicinity of the Fermi level. The spin-up bands show metallic feature, whereas the spin-down bands act as a semiconductor with an energy gap of about 0.97 eV. This points to the half-metallicity and ferromagnetic ground states of Fe-doped SMoSe JM. To give an insight into the spin-up states around the Fermi level, we calculate the total and projected density of states (DOS) of the doped JM, as shown in Fig. 2(a). From the under panel of Fig. 2(a), one can observe that the impurity states of the spin-up channel around the Fermi level arise primarily from Fe-*d* states, Mo-*d* states, and Se-*p* states.

Additionally, we carry out the Bader partial charge analysis to determine the bonding character and the charge of each ion in the doped SMoSe janus monolayer, and the results are given in Table 1. In Table 1, positive charge represents charge transfer from the atom, whereas negative charge means charge transfer to the atom. Mo and Cr atoms give away charges, while S and Fe atoms obtain charges. Hence, it could be concluded that Cr behaves like Mo while Fe behaves like an anion. Charge density distributions obtained in the best plane are given in Fig. 3, which verifies the behaviors of the ions in the Bader charge analyses.

Table 1
Bader partial net charges (in units of e) for Fe-doped SMoSe JM and Cr-doped SMoSe JM.

	Fe-doped SMoSe JM	Cr-doped SMoSe JM
S_1	−0.390	−0.393
S_2	−0.383	−0.391
S_3	−0.402	−0.396
S_5	−0.388	−0.390
S_6	−0.366	−0.392
S_9	−0.388	−0.392
S_{12}	−0.387	−0.388
Mo_2	0.646	0.660
Mo_3	0.672	0.687
Mo_4	0.644	0.652
Mo_5	0.648	0.660
Mo_6	0.674	0.675
Mo_7	0.660	0.668
Mo_8	0.663	0.660
Mo_9	0.675	0.666
Mo_{10}	0.674	0.674
Mo_{11}	0.661	0.670
Fe/Cr	−1.533	0.729

The calculated transmission spectrum of Fe-doped SMoSe JM homo-junction, as shown in the right panel of Fig. 1(b), displays a remarkable spin-splitting corresponding to the band structure of the left or right electrode. The spin-up channel is opened with two transmission peaks near the Fermi level, and the energy range of spin-up channel is between −0.34 eV and 0.13 eV. However, the spin-down channel is closed around the Fermi level. This indicates a single-spin conduction in this doped JM and provides a great reference for designing thermal related spin filter devices. It is worthwhile to note that the area of the spin-up channel below the Fermi level is more than that above the

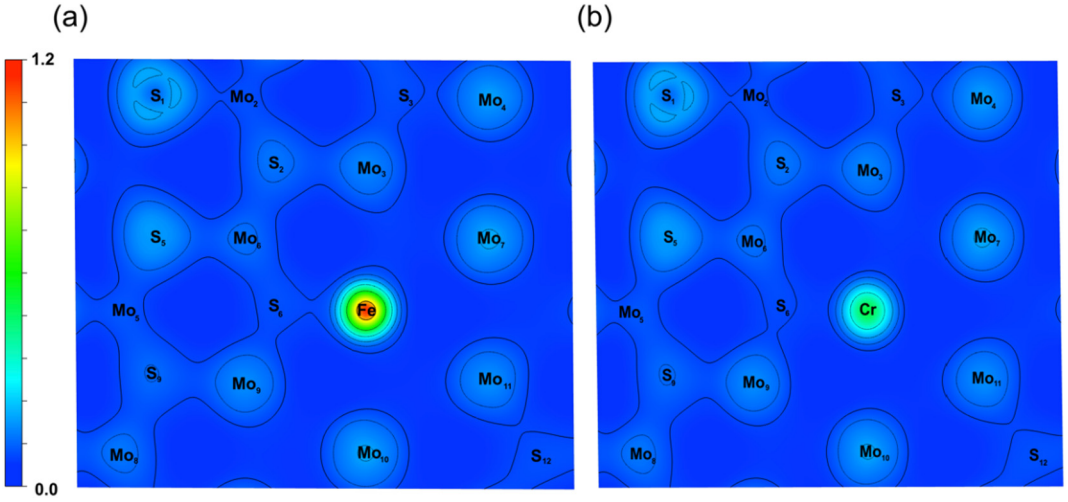

Fig. 3. The charge density distribution for Fe-doped SMoSe JM (a) and Cr-doped SMoSe JM (b).

Fermi level, which indicates that the spin-up hole carriers will dominate the thermal transport features. The spin-down channel of hole carriers is far away from the Fermi level, while that of the electrons is close to the Fermi level; hence, it is possible to excite the spin-down current if the temperature bias is higher than a given threshold.

To confirm the above-mentioned analysis, we now discuss the thermal induced spin current in this homo-junction. During the transport calculation, the current is driven by temperature bias (ΔT) without any external bias voltage, $\Delta T = T_L - T_R$, where T_L and T_R are the temperature of the source and drain, respectively. To understand the fundamental mechanism to generate spin current, we first look at the electron distribution in the source and drain. Fig. 4 shows the Fermi-Dirac distribution of the source (lower temperature) and drain (higher temperature). Since the source and drain of the homo-junction are the same material and have the same DOS, the difference of the carrier concentration between the source and drain is determined by the Fermi distribution ($f_L(E, T_L)$-$f_R(E,T_R)$), which is primarily related to the temperature of the two electrodes [15,35]. Electrons with energy higher than the Fermi level transport from the drain to the source, generating electron current I_e. At the same time, holes with energy lower than the Fermi level also flow from the drain to the source, giving rise to hole current I_h. If the system is highly spin-splitting, the spin currents are generated and flow in the opposite directions.

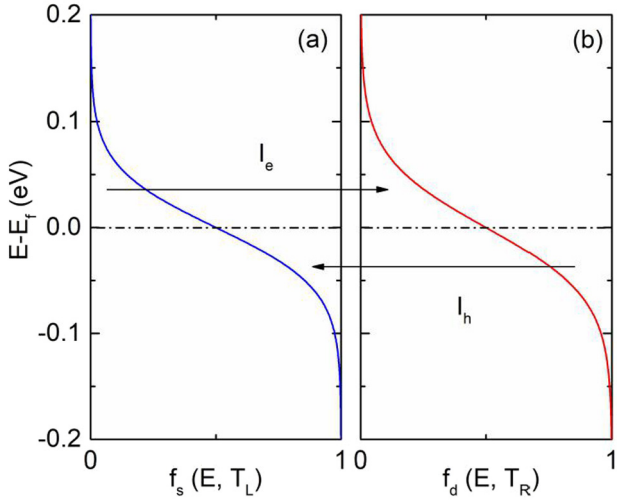

Fig. 4. The Fermi distribution of the source (left electrode with lower temperature) and drain (right electrode with higher temperature) of the homo-junction. When applying a temperature bias, the electron current flows from left to right, while the hole current flows in the opposite direction.

The thermal driven spin-dependent currents of the Fe-doped SMoSe JM homo-junction are shown in Fig. 5. Fig. 5(a) shows the calculated spin currents as a function of the source temperature T_L. The spin-up current (I_{up}) is negative, with remarkable values higher than previous Fe-doped MoS_2 monolayer device due to the larger span of the transport channel [16], while the spin-down (I_{dn}) current is nearly inhibited, which indicates a perfect thermal SFE in this system. The behavior of spin currents corresponds to the analysis of the transmission spectrum above. The negative spin-up current primarily originates from the hole carriers, which flow from the drain to source. The spin-up current increases with the increasing temperature bias (ΔT). It is interesting when the source temperature T_L is around 125 K, as the spin-up current increases to its maximum and then decreases, which indicates that a negative differential thermoelectric resistance [36] occurs in this thermal spin current. The thermal SFE is also observed in Fig. 5(b), which displays the spin currents with respect to temperature bias.

What's more, one can notice that the spin-down current, although still inhibited, increases slowly with the increase of temperature bias. This is due to the spin-down channel of electron carriers above the Fermi level, which gradually take part in transport when the temperature bias increases. The spin current can be further clarified from the current spectra $J(E) = T(E)(f(E, T_L)\text{-}f(E, T_R))$ [15,37], as show in Fig. 6(a). The area covered under the J(E) curves, associated with the axis of J(E) = 0, determines the magnitude of the spin current [15]. One can also find the inhibited spin-down channel and opened spin-up channel, confirming the emergence of the thermal SFE. Further, the larger area of spin-up current spectra below the Fermi level indicates that the spin-up current is dominated by hole carriers.

Now, we set out to discuss the results of Cr-doped SMoSe JM. The calculated band structure along the transport direction (Γ-Z) and corresponding transmission spectrum of its homo-junction are shown in Fig. 1(c). It is interesting that Cr-doped SMoSe JM is a typical spin-polarized semiconductor. The spin-splitting bands exhibit a finite band gap, and the spin-up and spin-down sub-bands are localized at the upside and downside of the Fermi level, respectively. It is important that these spin-splitting bands are localized around the Fermi level with nearly symmetrical dispersion and energy gaps, providing two spin-dependent transport channels: one for spin-up electrons, and the other for spin-down holes. This kind of band feature is important for the emergence of the SSE when a temperature bias is applied. The calculated DOS and projected DOS are also shown in Fig. 2(b), to give an insight into the spin states around the Fermi level. It is found that the spin states are mainly formed by the Cr-*d* states, Mo-*d* states and Se-*p*

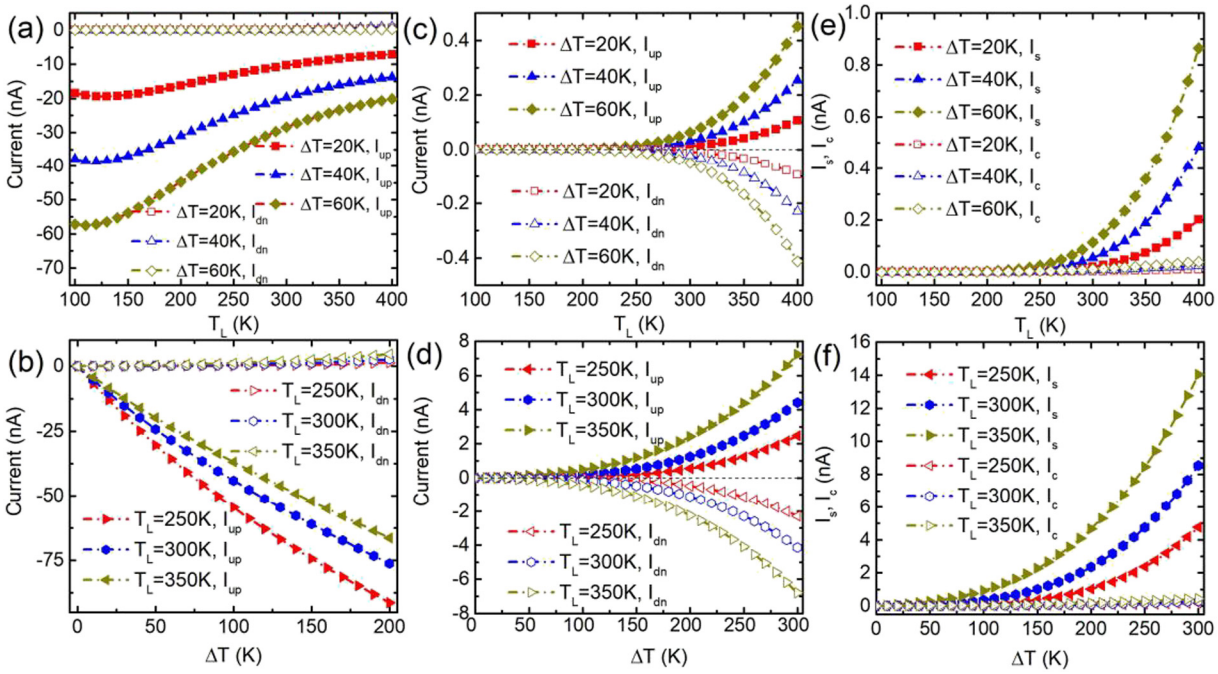

Fig. 5. Calculated spin-dependent currents generated by the temperature bias. (a) and (b) show the spin-dependent currents (I_{up} and I_{dn}) for Fe-doped SMoSe homo-junction as a function of the temperature of the source (T_L) and the temperature bias ΔT, respectively, where $\Delta T = T_L - T_R$. (c) and (d) denote spin-dependent currents for Cr-doped SMoSe homo-junction as a function of T_L and ΔT, respectively. (e) and (f) are the calculated total spin current (I_s) and charge current (I_c) for Cr-doped SMoSe homo-junction with respect to T_L and ΔT, respectively.

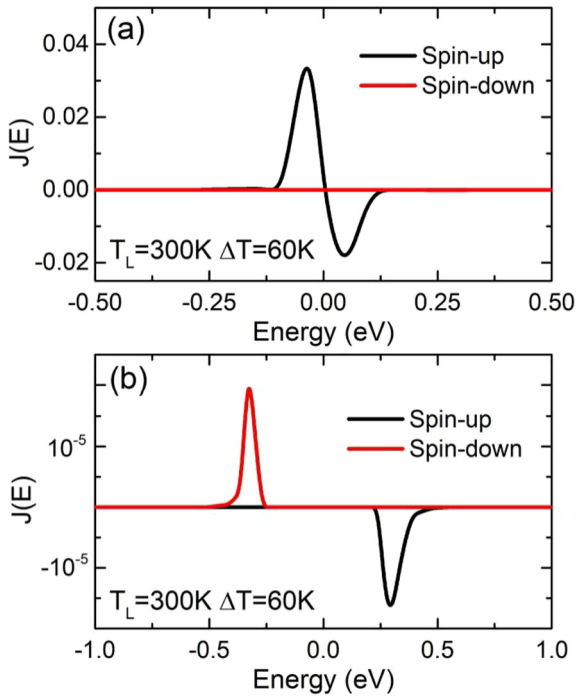

Fig. 6. The spin-dependent current spectra for Fe-doped SMoSe homo-junction (a) and Cr-doped SMoSe homo-junction (b) at (T_L = 300 K, ΔT = 60 K). The current spectra is calculated as $J(E) = T(E)(f(E, T_L)\text{-}f(E, T_R))$.

states.

The calculated transmission spectrum of the Cr-doped SMoSe homo-junction is shown in the right panel of Fig. 1(c). Corresponding to the band structure of the electrode, the spin-up and spin-down transmission channels are nearly symmetrical around the Fermi level. The spin-up channel is in the energy range of 0.24–0.56 eV, and the spin-down channel is in the energy range of (−0.26)–(−0.54) eV. From the formula of spin currents described in Eq. (1), the spin-dependent currents should be dominated by the net transmission around the Fermi level. Thus, when the device is placed in a temperature bias, it is possible to generate spin-dependent currents flowing in the opposite directions with nearly equal magnitude, and the SSE hence occurs. However, one can notice that the spin transmission channels have a wide energy gap with respect to the Fermi level. This indicates that the spin current could be driven after the temperature increases to a threshold.

To confirm these analyses, we also calculate the thermally driven spin-dependent currents through this Cr-doped SMoSe JM homo-junction, as shown in Fig. 5. Fig. 5(c) and (d) describe the spin currents of the homo-junction versus the temperature of source (T_L) and temperature bias (ΔT), respectively. It is clearly seen that the spin currents are generated via the temperature bias without any external bias voltage. The spin-up current is positive, while the spin-down current is negative, which are individually contributed by the spin-splitting electrons and holes flowing from the drain to source. Importantly, due to the symmetry of spin-up and spin-down transmission channels about the Fermi level, the spin-up and spin-down currents have nearly equal magnitudes and flow in the opposite directions. Since the spin currents are only generated by temperature bias, a perfect SSE thus emerges in this homo-junction, and Cr-doped SMoSe JM is therefore a promising candidate for spin caloritronics devices. From Fig. 5(c), we find a threshold temperature (T_{th}) of about 225 K. The spin currents are approximately zero when $T_L < T_{th}$, whereas the spin currents increase linearly with increasing T_L when $T_L > T_{th}$. This is due to the energy gap of transmission channels around the Fermi level, as discussed above. Fig. 5(d) shows that the spin currents increase with the increasing ΔT.

The advantage of SSE is the generation of pure spin current with overshadowed charge current, which is expected to reduce Joule heating and realize low-power-consumption devices [5,16,34]. To illuminate the perfect SSE, we investigate the thermal induced spin currents I_s (I_{up}-I_{dn}) and charge currents I_c (I_{up} + I_{dn}). Fig. 5(e) and (f) show the I_s (I_c) as a function of T_L and ΔT. One can clearly notice that

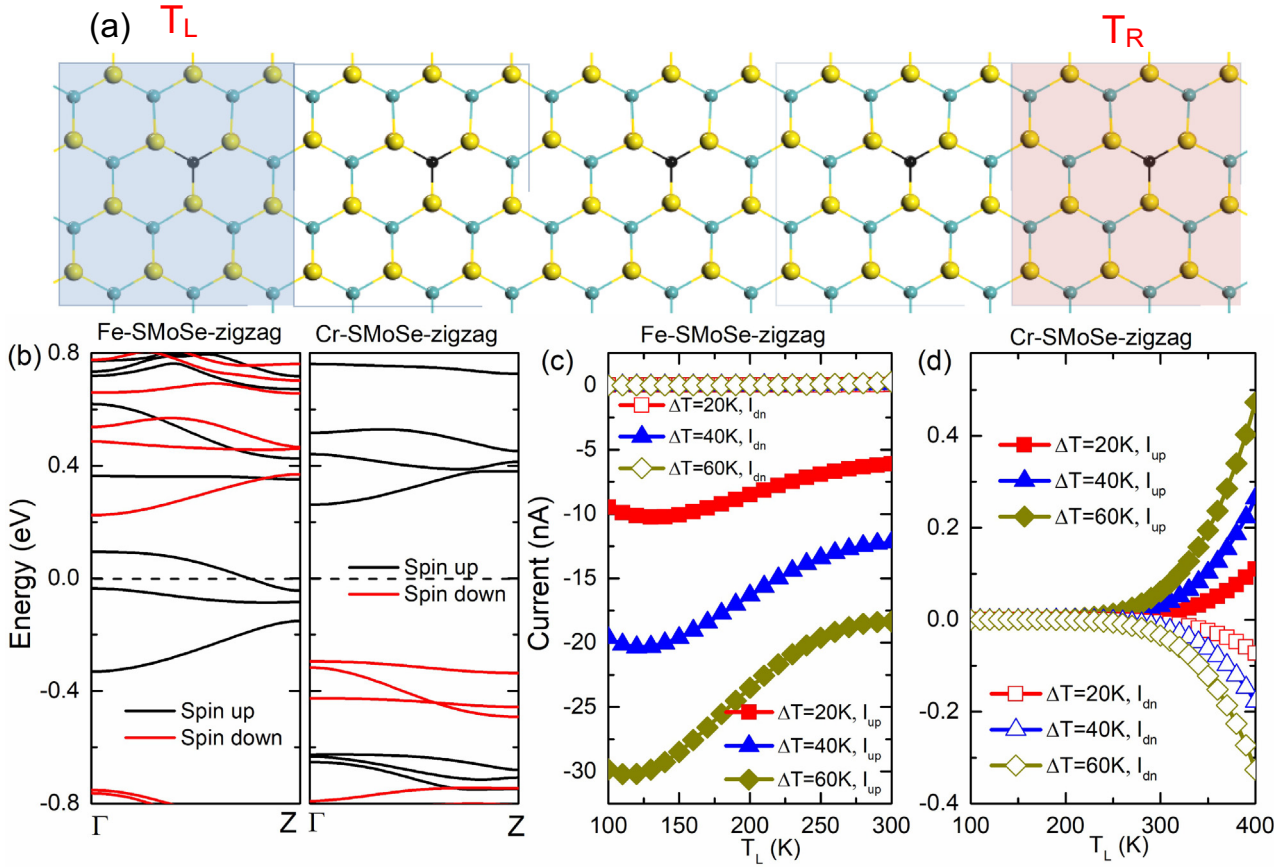

Fig. 7. Thermal spin transport properties of zigzag configuration of the device. (a) shows the schematic of the Fe(Cr)-doped SMoSe JM homo-junction with zigzag configuration. Calculated band structures of Fe- and Cr-doped SMoSe JMs along zigzag direction are shown in (b), (c) and (d) show the calculated spin-dependent currents in Fe- and Cr-doped SMoSe homo-junctions with zigzag configuration, respectively.

the charge currents are markedly inhibited, while the spin currents increase with increasing T_L or ΔT, which suggests that the spin currents dominate the thermal spin transport in the homo-junction. To further confirm the SSE, we also calculate the current spectra J(E) (T_L = 300, ΔT = 60) as shown in Fig. 6(b). Obviously, the spin-up current spectra is nearly symmetrical to the spin-down spectra about the Fermi level, with almost equal area associated with the axis of J = 0, further suggesting the emergence of a perfect SSE in this system.

One can notice that the results and discussions above are all based on armchair configuration of the devices. Is there any difference on the thermal spin transport properties when the devices are in zigzag configuration? At first, it is necessary to note that the doped SMoSe JMs are two-dimensional (2D) systems. Thus, no matter armchair or zigzag configuration of the devices, the magnetic features of their parent materials (doped SMoSe JMs) are not changed, which is different from the situation in one-dimensional nanoribbons [38]. To illustrate this point, we also calculated the band structures and spin-dependent currents of the doped JMs with a zigzag configuration of the device, as shown in Fig. 7. In Fig. 7(b), the band structures of the zigzag JMs exhibit the same properties as the armchair JMs, i.e., the half-metallic Fe-doped SMoSe JM and the spin-polarized semiconducting Cr-doped JM. Accordingly, calculated spin-dependent currents also exhibit the thermal SFE and SSE, as shown in Fig. 7(c) and (d), respectively. The difference in the magnitude of spin currents arises from the distinct band dispersion as originating from the structural anisotropy. Generally, no matter armchair or zigzag configuration of the devices, the intrinsic thermal spin transport properties are the same.

It is note-worthy that the Fe or Cr dope SMoSe JM proposed here could hopefully be fabricated in an experiment. Firstly, the SMoSe JM has already been synthesized experimentally [20]. Besides, modulating the properties of transition metal dichalcogenides via transition metal doping has already been achieved in experiments [21]. For example, Wang et al. studied the optical and electrical properties of Fe-doped MoS_2 layered crystals fabricated via a chemical vapor transport method [23]. Additionally, Cr-doped MoS_2 thin films were achieved by Lewis et al. [22] using an aerosol-assisted chemical vapor deposition method. Therefore, the Fe or Cr-doped SMoSe JM could be feasibly fabricated, and is for this reason a promising candidate for spin caloritronics.

4. Conclusion

In summary, using the density functional theory combined with non-equilibrium Green's function methods, we systematically studied the electronic structure of Fe(Cr)-doped SMoSe JM and spin-dependent thermal transport through the homo-junction. We have shown that the Fe-doped SMoSe JM is a ferromagnetic half-metal, while due to the unique spin-dependent band structures with a finite spin-splitting energy gap, the Cr-doped SMoSe JM behaves as a spin-polarized semiconductor. Calculated spin-dependent currents suggest a perfect thermal spin filter effect of Fe-doped SMoSe JM, and a negative differential thermoelectric resistance is also obtained in the thermal spin current. The two spin channels of Cr-doped SMoSe JM are highly symmetrical about the Fermi level, and the thermal induced spin-up and spin-down currents flow in opposite directions with nearly equal magnitude, producing a perfect spin Seebeck effect. Our findings show that these materials are promising candidates for spin caloritronics devices, such as thermal spin valves, spin Seebeck rectifiers or diodes, and thermal spin diodes with negative differential thermoelectric resistance.

Acknowledgments

This work is supported by National Natural Science Foundation of China (Grant No. 11804040 and 51801163) and Fundamental Research Funds for the Central Universities (Grant CQUPT: A2017-119).

References

[1] G.E. Bauer, E. Saitoh, B.J. van Wees, Spin caloritronics, Nat. Mater. 11 (2012) 391–399.
[2] S.R. Boona, R.C. Myers, J.P. Heremans, Spin caloritronics, Energy Environ. Sci. 7 (2014) 885–910.
[3] F. Mohmed, Y.H. Lin, Investigation of spin Seebeck effect and magnetic damping in nanometer thick $Ce_{0.5}Y_{2.5}Fe_5O_{12}$ films, Appl. Surf. Sci. 480 (2019) 1025–1034.
[4] M. Zeng, Y. Feng, G. Liang, Graphene-based spin caloritronics, Nano Lett. 11 (2011) 1369–1373.
[5] K. Uchida, S. Takahashi, K. Harii, J. Ieda, W. Koshibae, K. Ando, S. Maekawa, E. Saitoh, Observation of the spin Seebeck effect, Nature 455 (2008) 778–781.
[6] C.M. Jaworski, R.C. Myers, E. Johnston-Halperin, J.P. Heremans, Giant spin Seebeck effect in a non-magnetic material, Nature 487 (2012) 210–213.
[7] B.Z. Rameshti, A.G. Moghaddam, Spin-dependent Seebeck effect and spin caloritronics in magnetic graphene, Phys. Rev. B 91 (2015) 155407.
[8] H. Adachi, K. Uchida, E. Saitoh, S. Maekawa, Theory of the spin Seebeck effect, Rep. Prog. Phys. 76 (2013) 036501.
[9] X. Hao, J.S. Moodera, R. Meservey, Spin-filter effect of ferromagnetic europium sulfide tunnel barriers, Phys. Rev. B 42 (1990) 8235–8243.
[10] D.D. Wu, H.H. Fu, L. Gu, Y. Ni, F.X. Zu, K.L. Yao, Thermal spin filtering, thermal spin switching and negative-differential-resistance in thermal spin currents in zigzag SiC nanoribbons, Phys. Chem. Chem. Phys. 16 (2014) 17493–17498.
[11] A.V. Generalov, E.N. Voloshina, Yu.S. Dedkov, Structural and electronic properties of graphene-based junctions for spin-filtering: the graphene/Al/Ni(111) intercalation-like system, Appl. Surf. Sci. 267 (2013) 8–11.
[12] M. Hatami, G.E. Bauer, Q. Zhang, P.J. Kelly, Thermal spin-transfer torque in magnetoelectronic devices, Phys. Rev. Lett. 99 (2007) 066603.
[13] G. Gao, G. Ding, J. Li, K. Yao, M. Wu, M. Qian, Monolayer MXenes: promising half-metals and spin gapless semiconductors, Nanoscale 8 (2016) 8986–8994.
[14] J. He, S. Li, Two-dimensional Janus transition-metal dichalcogenides with intrinsic ferromagnetism and half-metallicity, Comput. Mater. Sci. 152 (2018) 151–157.
[15] H.H. Fu, D.D. Wu, Z.Q. Zhang, L. Gu, Spin-dependent Seebeck effect, thermal colossal magnetoresistance and negative differential thermoelectric resistance in zigzag silicene nanoribbon heterojunciton, Sci. Rep. 5 (2015) 10547.
[16] F. Zou, L. Zhu, G. Gao, M. Wu, K. Yao, Temperature-controlled spin filter and spin valve based on Fe-doped monolayer MoS_2, Phys. Chem. Chem. Phys. 18 (2016) 6053–6058.
[[17] D.D. Wu, Q.B. Liu, H.H. Fu, R. Wu, How to realize a spin-dependent Seebeck diode effect in metallic zigzag γ-graphyne nanoribbons? Nanoscale 9 (2017) 18334–18342.
[18] D.-D. Wu, H.-H. Fu, Q.-B. Liu, G.-F. Du, R. Wu, Magnetic nanotubes: a new material platform to realize a robust spin-Seebeck effect and a perfect thermal spin-filtering effect, Phys. Rev. B 98 (2018) 115422.
[19] V. Musle, A. Kumar, S. Choudhary, Temperature dependent spin transport investigations in single layer VTe_2, J. Alloy. Compd. 770 (2019) 345–349.
[20] J. Zhang, S. Jia, I. Kholmanov, L. Dong, D. Er, W. Chen, H. Guo, Z. Jin, V.B. Shenoy, L. Shi, J. Lou, Janus monolayer transition-metal dichalcogenides, ACS Nano 11 (2017) 8192–8198.
[21] A.A. Tedstone, D.J. Lewis, P. O'Brien, Synthesis, properties, and applications of transition metal-doped layered transition metal dichalcogenides, Chem. Mater. 28 (2016) 1965–1974.
[22] D.J. Lewis, A.A. Tedstone, X.L. Zhong, E.A. Lewis, A. Rooney, N. Savjani, J.R. Brent, S.J. Haigh, M.G. Burke, C.A. Muryn, J.M. Raftery, C. Warrens, K. West, S. Gaemers, P. O'Brien, Thin films of molybdenum disulfide doped with chromium by aerosol-assisted chemical vapor deposition (AACVD), Chem. Mater. 27 (2015) 1367–1374.
[23] S.Y. Wang, T.S. Ko, C.C. Huang, D.Y. Lin, Y.S. Huang, Optical and electrical properties of MoS_2 and Fe-doped MoS_2, Jpn. J. Appl. Phys. 53 (2014) 04EH07.
[24] J.P. Perdew, K. Burke, M. Ernzerhof, Generalized gradient approximation made simple, Phys. Rev. Lett. 77 (1996) 3865–3868.
[25] G.F. Kresse, J. Furthmüller, Efficient iterative schemes for *ab initio* total-energy calculations using a plane-wave basis set, Phys. Rev. B 54 (1996) 11169.
[26] G. Henkelman, A. Arnaldsson, H. Jónsson, A fast and robust algorithm for Bader decomposition of charge density, Comput. Mater. Sci. 36 (2006) 354–360.
[27] R.F.W. Bader, Atoms in Molecules: A Quantum Theory, Clarendon, Oxford, 1990.
[28] M. Brandbyge, J.L. Mozos, P. Ordejo'n, J. Taylor, K. Stokbro, Density-functional method for nonequilibrium electron transport, Phys. Rev. B 65 (2002) 165401.
[29] J.M. Soler, E. Artacho, J.D. Gale, A. Garcıa, J. Unquera, P. Ordejon, D. Sanchez-Portal, The SIESTA method for ab initio order-N materials simulation, J. Phys. Condens. Matter 14 (2002) 2745–2779.
[30] J. Taylor, H. Guo, J. Wang, *Ab initio* modeling of quantum transport properties of molecular electronic devices, Phys. Rev. B 63 (2001) 245407.
[31] M. Büttiker, Y. Imry, R. Landauer, S. Pinhas, Generalized many-channel conductance formula with application to small rings, Phys. Rev. B 31 (1985) 6207–6215.
[32] Y. Imry, R. Landauer, Conductance viewed as transmission, Rev. Mod. Phys. 71 (1999) S306–S312.
[33] Y.C. Cheng, Z.Y. Zhu, W.B. Mi, Z.B. Guo, U. Schwingenschlögl, Prediction of two-dimensional diluted magnetic semiconductors: doped monolayer MoS_2 systems, Phys. Rev. B 87 (2013) 100401.
[34] M.D. Xie, C.G. Tan, P. Zhou, J.D. Lin, L.Z. Sun, Ferrimagnetic half-metallic properties of Cr/Fe δ doped MoS_2 monolayer, RSC Adv. 7 (2017) 20116–20122.
[35] Y. Ni, K. Yao, H. Fu, G. Gao, S. Zhu, S. Wang, Spin seebeck effect and thermal colossal magnetoresistance in graphene nanoribbon heterojunction, Sci. Rep. 3 (2013) 1380.
[36] K. Kobashi, R. Hayakawa, T. Chikyow, Y. Wakayama, Negative differential resistance transistor with organic p-n heterojunction, Adv. Electron. Mater. 3 (2017) 1700106.
[37] L. Zhu, R.M. Li, K.L. Yao, Temperature-controlled colossal magnetoresistance and perfect spin Seebeck effect in hybrid graphene/boron nitride nanoribbons, Phys. Chem. Chem. Phys. 19 (2017) 4085–4092.
[38] F. Meng, X. Chen, S. Sun, J. He, Electronic and magnetic properties of pristine and hydrogenated borophene nanoribbons, Phys. E. 91 (2017) 106–112.